UNIVERSITY OF BATH

Citation for published version:
Ndi, M, Masuyer, G, Dawitz, H, Carlström, A, Michel, M, Elofsson, A, Rapp, M, Stenmark, P & Ott, M 2019, 'Structural basis for the interaction of the chaperone Cbp3 with newly synthesized cytochrome b during mitochondrial respiratory chain assembly', *Journal of Biological Chemistry*.
https://doi.org/10.1074/jbc.RA119.010483

DOI:
10.1074/jbc.RA119.010483

Publication date:
2019

Document Version
Peer reviewed version

Link to publication

University of Bath

Structural basis for the interaction of the chaperone Cbp3 with newly synthesized cytochrome *b* during mitochondrial respiratory chain assembly

Mama Ndi[1*], Geoffrey Masuyer[1,2*], Hannah Dawitz[1*], Andreas Carlström[1], Mirco Michel[1,3], Arne Elofsson[1,3], Mikaela Rapp[1], Pål Stenmark[1,4, §], and Martin Ott[1,§]

[1] Department of Biochemistry and Biophysics, Stockholm University, SE-10691 Stockholm, Sweden; [2] Department of Pharmacy and Pharmacology, University of Bath, Bath BA2 7AY, UK; [3] Science for Life Laboratories, Stockholm University, SE-171 21 Solna, Sweden; [4] Department of Experimental Medical Science, Lund University, SE-221 84 Lund, Sweden.

Running title: Structure-function of Cbp3

[§], please address correspondence to MO or PS: martin.ott@dbb.su.se, +46-8162461; stenmark@dbb.su.se, +46-8163729

[*], these authors contributed equally to this work

Abstract

Assembly of the mitochondrial respiratory chain requires the coordinated synthesis of mitochondrial and nuclear encoded subunits, redox co-factor acquisition, and correct joining of the subunits to form functional complexes. The conserved Cbp3–Cbp6 chaperone complex binds newly synthesized cytochrome *b* and supports the ordered acquisition of the heme co-factors. Moreover, it functions as a translational activator by interacting with the mitoribosome. Cbp3 consists of two distinct domains, an N-terminal domain present in mitochondrial Cbp3 homologs, and a highly conserved C-terminal domain comprising a ubiquinol–cytochrome *c* chaperone region. Here, we solved the crystal structure of this C-terminal domain from a bacterial homolog at 1.4 Å resolution, revealing a unique all-helical fold. This structure allowed mapping of the interaction sites of yeast Cbp3 with Cbp6 and cytochrome *b* via site-specific photo-crosslinking. We propose that mitochondrial Cbp3 homologs carry an N-terminal extension that positions the conserved C-terminal domain at the ribosomal tunnel exit for an efficient interaction with its substrate, the newly synthesized cytochrome *b* protein.

Introduction

The inner mitochondrial membrane contains the respiratory chain complexes that, in ensemble, transfer electrons extracted from metabolites to the ultimate acceptor O_2. The bc_1 complex (Complex III) plays a central role in this pathway and shuttles electrons from reduced ubiquinol to cytochrome *c*. The bc_1 complex consists of nine nuclear subunits and the mitochondrially encoded cytochrome *b* (Cyt*b*), which, together with cytochrome c_1 and the Rieske iron-sulfur protein, forms the catalytic center (1). Synthesis and assembly of the bc_1 complex (Fig. 1A) starts with the translation of the messenger RNA for Cyt*b* (*COB* mRNA) on the mitochondrial ribosome (mitoribosome) (2,3). The translational activators Cbp1, Cbs1 and Cbs2 help in stabilizing and binding the *COB* mRNA on the mitoribosome (4), and together with the Cbp3-Cbp6 complex bound in close proximity to the polypeptide tunnel exit (PTE), translation of the Cyt*b* transcript is initiated (5). Cyt*b* interaction with Cbp3-Cbp6 leads to a release of the complex from mitoribosomes (5) to establish the first assembly intermediate of the bc_1 complex. The incorporation of a low potential heme group at the b_L site of Cyt*b* triggers the binding of Cbp4 to Cyt*b* (intermediate I) (6), which accumulates to well-detectable levels in wild type cells (6,7). Upon incorporation of the second heme group at the b_H site, the Cbp3-Cbp6 complex is released from the fully hemylated Cyt*b* and returns to the mitoribosome to initiate another round of *COB* mRNA translation (6,7). In cases when the Cbp3-Cbp6 complex is not released from assembly intermediate I, it is unavailable to stimulate new rounds of *COB* mRNA translation. The Cbp3-

1

Cbp6 complex, therefore, plays a dual role in this process as it controls both Cyt*b* translation and assembly (7). Consequently, the respiratory deficiencies of strains lacking Cbp3 or Cbp6 are due to inefficient *COB* mRNA translation and bc_1 complex assembly (5). Furthermore, knock down of the human Cbp3 homolog UQCC1 leads to loss of the human Cbp6 homolog UQCC2 and reduced levels of assembled bc_1 complex (8).

Therefore, Cbp3-Cbp6 comprise a protein complex that interacts with its substrate Cyt*b* in a context-dependent fashion. It shares this behavior with other assembly factors of the respiratory chain (9-11). However, the understanding of how these mitochondrial respiratory chain assembly factors work is limited. The mitochondrial Cbp3 protein contains two domains, an N-terminal domain present in mitochondria and a highly conserved ubiquinol-cytochrome *c* chaperone domain, which is also found in Cbp3 homologs in bacteria. Here, we present the crystal structure of a Cbp3 protein from the bacteria *Brucella abortus (Ba*Cbp3) at 1.4Å resolution. The protein has a unique, all-helical fold that was solved using *ab initio* phasing. Homology modeling and biochemical analysis of Cbp3 from *Saccharomyces cerevisiae* (*Sc*Cbp3) allowed us to map the molecular interactions of *Sc*Cbp3 with Cbp6 and Cyt*b*.

Results

Bioinformatics and biochemical analysis of the domain structure of yeast Cbp3

Cbp3 is a key assembly factor of Cyt*b* that plays an additional role in regulating translation of *COB* mRNA. To understand how Cbp3 operates, we aimed at determining its structure and interactions sites with other proteins. We first set out to identify conserved domains. Using *Sc*Cbp3 (UniProt #P21560) as a representative of this structurally uncharacterized family, multiple sequence alignments were generated at different sensitivity cut-offs, using HHblits and Jackhmmer (12),(13). With the most permissive sensitivity cut-off (E-value = 1), 649 and 740 sequences were reported in HHblits and Jackhmmer, respectively (Fig. 1B). Results from PSIPRED classifies Cbp3 as an all-alpha fold protein, with twelve alpha helices predicted (Fig. S1A). Two domains were identified, a conserved C-terminal domain spanning residues 140-290, annotated as ubiquinol-cytochrome *c* chaperone

domain, and a variable N-terminal domain of unknown function spanning residues 61-119 (Fig. 1B), which is present only in mitochondrial Cbp3 homologs.

To identify the importance of the different domains, we constructed strains expressing either only the N-terminal domain of Cbp3 (Cbp3_1-120) or only the C-terminal domain (Cbp3_120-335 or Cbp3_145-335) fused with the N-terminal presequence of Oxa1 allowing it to be targeted to mitochondria. In absence of Cbp3, cells cannot respire, while expression of Cbp3 from a plasmid rescued the phenotype (Fig. 1C). Expression of the truncated forms of Cbp3 did not restore the respiratory growth of the *cbp3Δ* strain (Fig. 1C). Previous studies showed that Cbp6 is unstable in the absence of Cbp3 (5). Therefore, we tested the protein levels of the truncated Cbp3 mutants and protein levels of Cbp6 in the Cbp3 mutants. Only low amounts of the N-terminal domain were detected while the conserved C-terminal domain was not stable (Fig 1D). Furthermore, expression of the Cbp3 mutants could not rescue Cbp6 protein levels.

Brucella abortus Cbp3 as a structural template for mitochondrial Cbp3

Our bioinformatic analysis showed that Cbp3 homologs from alpha-proteobacteria are most closely related to *Sc*Cbp3. We recombinantly expressed and purified the Cbp3 homolog of *Brucella abortus,* an alpha-proteobacterium, which has 22% sequence identity. The structure was solved using *ab-initio* phasing and refined at 1.4 Å resolution (Tab. 1). Structure determination was facilitated by the predicted high α-helical content, which revealed a compact helical bundle with a unique fold (Fig. S1B). A search of the PDB using PDBeFOLD (14) confirmed that the Cbp3 fold was not previously described, the top hits had RMSD values above 4Å and only superimposed a few helices. Residues 1-181 were modelled in the high-resolution density map, with only three carboxy–terminal residues missing from the structure (181-184; Fig. 2). Of note, two magnesium ions were bound to *Ba*Cbp3, which likely originated from the crystallization condition (Fig. 2A, C, D). The core of *Ba*Cbp3 consists of nine helices with the long N-terminal helix protruding from the rest of the protein (Fig. 1B; Fig. S1C). Although *Ba*Cbp3 is monomeric, strong hydrophobic interactions were observed between the aliphatic residues of the N-terminal

2

helix (Fig. 2B), and a shallow pocket of the symmetry-related molecule on the opposite side, formed by the base of helices 4, 5 and 6 (Fig. S1D, G). The core of the protein is formed by a deep hydrophobic pocket which is rich in aromatic residues (F33, Y34, Y115, Y151), including a central histidine (H53). This pocket is highly conserved in ScCbp3 (F143, Y144, Y228, Y265 and H163; Fig. 3C).

Interestingly, the two magnesium ions are located in a large cavity with a negatively charged surface (Fig. 2B-D). The two ions present a typical octahedral coordination (Fig 2C, D; Fig. S1E, F). On one site, Mg^{2+} coordination is mediated by D82, S86, and E89 interactions with water molecules. On the second site, E74 directly interacts with Mg^{2+}, which is further stabilized by water-mediated interactions with E14, D77 and E78. Although the presence of Mg^{2+} suggests a possible metal-binding motif, no physiological function could be associated with magnesium. Likewise, residues D82 (Sc D193) and E89 (Sc E201) are highly conserved, while the other residues are variable (Fig. 3A, C, D).

The new fold presented by BaCbp3 was used as a template to further investigate the properties of the Cbp3 family, and more particularly to determine protein contacts of Cbp3. A homology model of the yeast Cbp3 (ScCbp3) was calculated (15). The resulting model of the yeast ubiquinol-cytochrome c chaperone domain corresponded to residues 115-294 (Fig. 1A, 3B-D), therefore missing most of the N-terminal domain which is only conserved in mitochondrial homologs (Fig. 1B). The core of the protein is very similar to BaCbp3 with the central hydrophobic residues showing strong conservation (Fig. 3A, C). The surface potential of the ScCbp3 model presents a similar profile to BaCbp3 (Fig. 2B, 3D), although the negatively charged cavity that holds the Mg^{2+}-binding sites in BaCbp3 is less prominent and appears substantially more shallow and hydrophobic in ScCbp3.

Interaction sites of Cbp3 with Cbp6 and Cytb in Sacharomyces cerevisiae

The homology model of ScCbp3 enabled us to identify surface-exposed residues that could be part of a protein-protein interaction surface with either Cbp6, Cyt$b$, the mitochondrial ribosome or other interaction partners. Therefore, we aimed to identify these protein contacts by site-directed photocrosslinking (16), which detects contacts of

proteins within an amino-acid range. Tagged variants of Cbp3 (Cbp3His7) were constructed by changing of selected codons to an amber stop codon. These Cbp3 variants were then overexpressed in a $cbp3\Delta$ yeast strain, which in parallel expressed the aminoacyl-synthetase/tRNA pair allowing to incorporate the photo-activatable amino acid para-aminobenzoylphenylalanine (pBpa) at these amber stop codons. Supplementing the growth medium with pBpa enabled incorporation of this amino acid at the desired position and the formation of specific crosslinking products upon irradiation (Fig. 4B). 23 positions in Cbp3 were chosen (Fig. 4C), cells were subjected to UV irradiation and proteins analyzed by SDS-PAGE. Western blotting against Cbp3 showed a plethora of crosslink products with different sizes (Fig. 4D).

Next, we set out to determine specific crosslink partners of Cbp3 via Western blotting. Four residues that together contained all crosslinking products were chosen, namely positions K177, D188, R245 and K252. The cells were grown in the presence of pBpa, UV-irradiated and the crosslink products were purified via a C-terminal 7x-His-tag on Cbp3. Positions R245[pBpa] and K252[pBpa] showed a strong crosslink product with a 15-18 kDa partner, which we identified to be Cbp6 (Fig. 4D-E; Fig. S2B), in line with the previously described tight binding of Cbp3 and Cbp6 (5). To pinpoint an interaction surface of Cbp3 with Cbp6, we repeated the crosslink screen of all positions decorating against Cbp6. In this way, we identified four positions, K148[pBpa], P150[pBpa], R245[pBpa] and K252[pBpa], showing a strong crosslink with Cbp6 (Fig. S2B). The identified positions were subsequently mapped on the surface of the ScCbp3 model and were consistent with a large interaction site with Cbp6 (Fig. 4F).

Previous studies showed that the Cbp3-Cbp6 complex binds to the mitoribosome in close proximity to Mrpl4 (uL29m) (5). Since Mrpl4 is adjacent to the tunnel exit proteins Mrpl22 (uL22m), Mrp20 (uL23m), Mrpl40 (uL24m) and Mrpl3 (mL44) of the mitoribosome (17-19) and Cbp3 contacts Cyt$b$ when it is emerging from the tunnel exit, we set out to find an interaction site of Cbp3 with the mitoribosome. Cbp3 forms two crosslinking products around the size of 77 and 86 kDa, which could represent this interaction site based on the apparent molecular weight of Mrpl3, Mrp20, Mrpl22, Mrpl40 and Mrpl4 (44, 31, 35,

3

34 and 37 kDa, respectively). We tested various positions facing different sides of the protein, but we could not identify any interaction site of the C-terminal domain of Cbp3 with the mitoribosome (Fig. S2C, D). These negative results could be explained by shortcomings in the methods, because site-directed photocrosslinking can be sensitive to the local amino acid context, which would obstruct crosslinking. Alternatively, it is possible that the interaction between Cbp3 and the mitoribosome is instead mediated by the N-terminal domain and/or Cbp6.

Having identified the Cbp6-binding site, we explored further interaction sites with Cbp3 interactors. Cbp3 plays an important role in the assembly of the bc_1 complex by stabilizing newly synthesized Cyt$b$. Thus, we aimed to find the interaction site of Cbp3 with Cyt$b$. To increase sensitivity, we performed *in vivo* labeling of mitochondrially encoded translation products with radiolabeled [^{35}S]-methionine prior to UV-crosslinking and denaturing Cbp3His7 purification. Detection of the radioactivity showed a crosslink product of 64 kDa at the positions Q183, K185, D188, E195 and K215 (Fig. 4H). Western blotting confirmed that the crosslink product at D188[pBpa] contained both Cyt$b$ and Cbp3 (Fig. 4 G, H). Cyt$b$, and especially its matrix facing loops, are overall positively charged, but contain also three aspartic acid and one glutamic acid residue (20) enabling the interaction of acidic residues like D188 and E195 as well of basic residues like K185 and K215 of Cbp3 (Fig. 4I). Taken together, the Cyt$b$ interaction surface is situated adjacent, but not overlapping with the interaction site with Cbp6. This presumably allows the protein to contact simultaneously Cbp6 and newly synthesized Cyt$b$.

Discussion

In this study, we determined the structure of the conserved ubiquinol-cytochrome c chaperone domain of ScCbp3 and identified its functions in the biogenesis of the bc_1 complex. Previous studies provided evidence that Cbp3 and Cbp6 form a complex, which is involved in the synthesis of Cyt$b$ and the early assembly of the bc_1 complex in yeast (7). For an efficient synthesis of Cyt$b$, the Cbp3-Cbp6 complex interacts with the tunnel exit of the mitoribosome, where the complex binds the newly synthesized

Cyt$b$ (5). Mitochondrial Cbp3 homologs contain a highly conserved ubiquinol-cytochrome c chaperone domain at the C-terminus of unknown structure, while a domain without annotated function is found at the N-terminus. By expressing the domains of Cbp3 individually, we showed that neither domain is sufficient to restore respiration in strains lacking a full length Cbp3. To analyze protein contacts of the conserved C-terminus, we solved the structure of a Cbp3 homolog from *Brucella abortus* of the alpha-proteobacteria clade, which are the evolutionary closest relatives to mitochondria.

Despite differences in the amino acid sequences, the yeast and bacterial homologs are expected to present a common overall fold of the conserved ubiquinol-cytochrome c chaperone domain. A homology model of ScCbp3 enabled us to select potential sites of interactions with components of the bc_1 complex, the translational machinery or other unknown interaction partners. By incorporating a photo-reactive amino acid (pBpa) at specific positions of Cbp3, we could investigate interactions with high precision. We identified two main protein interaction sites on ScCbp3, which involve a hydrophobic and a positively charged surface on opposite sides of Cbp3 (Fig. 5). The Cbp3-Cbp6 interface is formed by a positive protrusion formed by a long flexible loop and a more stringent shorter loop (K148, P150, R245, K252; Fig. S1C). Unfortunately, there is no structure information available for Cbp6, but it is likely that a negatively charged pocket in Cbp6 enables binding to Cbp3. Interestingly, one position adjacent to the protrusion, R151, does not crosslink to Cbp6 (Fig. S2B). Our Cbp3 model shows that this residue instead most likely interacts with other negatively charged amino acids within the protein (E132, E145), maybe stabilizing the loop, and is therefore not available to interact with Cbp6. The interaction site of Cbp3 with Cyt$b$ is quite large, which fits well to the highly flexible matrix facing loops of Cyt$b$. These loops are overall polar or positively charged, but also include a few acidic residues enabling interactions with negative amino acids (D188 and E195) as well as basic (K185 and K215) and polar residues (Q183).

Interestingly, Cbp3 functions as an assembly factor as well as a translational activator in mitochondria. Since the N-terminus of Cbp3 is specific to mitochondrial Cbp3 homologs, it is tempting to speculate that this domain mediates

contacts with the mitoribosome and its bound Cbp6. In turn, Cbp6 is only stable in the presence of Cbp3 and a small fraction of overexpressed Cbp6 can interact with the ribosome in absence of Cbp3 (5). The interaction between Cyt*b* and Cbp3 is only transient to stabilize the Cyt*b* until other subunits join in the assembly intermediates (5-7). Likewise, the interaction between Cbp3-Cbp6 and the mitoribosome occurs only when Cbp3-Cbp6 is not bound to Cyt*b*. These context-dependent interactions likely require profound flexibility in Cbp3-Cbp6 to enable conformational changes preparing the proteins for binding the different clients. It will therefore be important to reveal the structure of Cbp3-Cbp6 either in its free form, in complex with Cyt*b* or the mitoribosome to unravel possible conformational changes induced by substrate binding.

Experimental procedures

Bioinformatics analysis of *Sc*Cbp3

Cbp3 from *Saccharomyces cerevisiae* was used as the reference sequence. HHblits and Jackhmmer were used to search the input sequence against the latest HHblits database and Uniref100, respectively. At E-value = 1, HHblitts reported 649 sequences while Jackhmmer gave 740. Possible contacts between pairs of amino acids in Cbp3 were predicted using Pconsc2 and the resultant map displayed a clear signal between residue 140 and 290. Pfam classified this region as an ubiquinol-cytochrome *c* chaperone domain. We used Pconsfold and Rosetta to predict the model while the quality of the model was assessed using Molprobity. The crystal structure of BaCbp3 was used as a template to produce the final homology model of ScCbp3 in SWISS-MODEL (15).

Cbp3 protein production and purification

The Cbp3 homologous sequence from *B. abortus* was cloned into the pET28a vector, containing a TEV-cleavable C-terminal GFP-His$_7$ tag. The vector was transformed into BL21 (DE3) *E. coli* strain and grown in fresh Terrific Broth medium, supplemented with kanamycin (50 µg/ml) at 180 rpm and 37ºC. Protein expression was induced when the culture was at an optical density of 0.8, by addition of 0.5 mM isopropyl ß-D-1-thiogalactopyranoside (IPTG) while the incubation temperature was reduced to 16ºC and

cultured for 18 h. Cells were harvested at 4°C, 6.500xg for 15 min using rotor JLA 8.1000. The cell pellet was re-suspended in lysis buffer (300 mM NaCl, 20 mM HEPES, 3 mM DTT, complete protease inhibitor (1 tablet per 20 grams of cell mass, Roche) and 1 mM MgSO$_4$) and drops of the suspension were flash frozen in liquid nitrogen. Frozen cells were lysed using Cryo Mill (MM400, Retsch) and the lysate was homogenized in appropriate amount of the lysis buffer. Cell debris was removed by centrifugation at 40.000xg for 20 min at 4ºC. The supernatant was adjusted to a final concentration of 10 mM imidazole and incubated with 1 mg of Ni-NTA Superflow resin (Qiagen) per 20 mg of GFP-His$_7$ for 4 h, at 4ºC. The slurry was transferred into a glass Econo-Column (Bio-Rad) and washed in the lysis buffer for 2 x 20 column volumes at 20 and 40 mM imidazole, respectively. Two column volumes of lysis buffer containing 250 mM imidazole was used to elute the Cbp3-GFP-His$_7$ fusion from the column. The eluate was dialysed overnight in the presence of 1 mg of TEV-protease per 10 mg of fusion protein, in 3L of buffer (20 mM HEPES, pH 7.4, 300 mM NaCl and 3 mM DTT). After dialyses the sample was passed through a 5 mL bed volume Ni-NTA His-Trap Column (GE Healthcare) and Cbp3 with residual residues of the TEV site after cleavage was collected in the flow through. Relative molecular mass of 10 kDa cutoff concentrators were used to concentrate the protein. The protein solution was then loaded onto a Superdex 200 10/300 gel-filtration column (GE Healthcare) which was equilibrated with buffer (300 mM NaCl, 20 mM HEPES, 3 mM DTT). From the chromatogram, fractions of the pure protein were pooled and concentrated to 25 mg/mL and used to set up crystallization trials.

X-ray crystallography

Crystals were obtained from a sitting-drop in 20% v/v polyethylene glycol 8000, 0.1 M TRIS pH 8.0, 0.2 M magnesium chloride hexahydrate. A drop of 200 nl of sample was mixed with equal amount of reservoir and incubated at 16°C, were crystals grew within 24h. Crystals were transferred briefly into a cryo-protectant solution, consisting of their respective growth condition supplemented with 20% glycerol, before freezing in liquid nitrogen.

Diffraction data were collected at station I04-1 of the Diamond Light Source (Oxon, UK), equipped with a PILATUS-6M detector (Dectris, Switzerland). Complete datasets to a resolution of

1.42 Å were collected from a single crystal at 100 K. Raw data images were processed and scaled with DIALS (21), and AIMLESS (22) using the CCP4 suite 7.0 (23). The resolution cut-off chosen was based on the $CC_{1/2}$ (24).

Initial phases for structure solution of *Ba*Cbp3 were obtained with ARCIMBOLDO Lite (25,26) by setting a search mode for multiple helices of 15 residues. The resulting model consisted of 7 fragments for a total of 150 poly-alanine residues traced (Fig S3). The model was manually curated and correctly place residues were used as a search model in PHASER (27) followed by partial building with BUCCANEER (28). The working model was refined using REFMAC5 (29) and manually adjusted with COOT (30). Water molecules were added at positions where Fo−Fc electron density peaks exceeded 3σ, and potential hydrogen bonds could be made. Validation was performed with MOLPROBITY (31). Ramachandran statistics show that 98% of all residues were in the most favoured region, and none in the disallowed region. Crystallographic data statistics are summarized in Table 1. Figures were made with PyMOL (Schrödinger, LLC, New York).

Plasmid construction

Cbp3 variants containing an amber stop codon (TAG) at selected sites were constructed by site directed mutagenesis (Supplemental Table) using a pGEM3 vector (Promega). The Cbp3 variants were later cloned into pYX142 (Novagen) using the restriction enzymes NcoI and HindIII.

To express EcYRS-Bpa (modified *E. coli* tyrosyl-tRNA synthetase) and tRNA (*E. coli* tyrosyl tRNA$_{CUA}$) for UV-crosslink experiments, EcYRS-Bpa and tRNA$_{CUA}$ were amplified from pESC-ECYRS-Bpa (16) and cloned into pRS403 (Nova lifetech) using the restriction sites XbaI and SapI. The plasmid was cut within the *HIS* gene with NdeI for integration into the yeast genome.

To express the C-terminal domain of Cbp3 the respective domain (Cbp3_120-335, Cbp3_145-335) was amplified by PCR and cloned with NotI and XhoI into a pYX132 plasmid containing the mitochondrial targeting sequence of Oxa1 (MTS_1-48) to ensure import. The N-terminal domain (Cbp3_1-120) was cloned with NotI and XhoI into pYX132.

Yeast strain construction

All yeast strains were isogenic to W303 (MATa *leu2-3,112 trp1-1 can1-100 ura3-1 ade2-1 his3-11,15*). The plasmid harboring the pBpa-RS and tRNA$_{CUA}$ was integrated into the genome of a strain lacking *CBP3*. In parallel this strain was transformed with pYX142 containing the respective variants of Cbp3. The obtained strains were grown on minimal medium lacking leucine (Sigma Y1376) and supplemented with 2% galactose (SGal-Leu) in the presence or absence of pBpa (p-benzoyl-L-phenylalanine).

Growth assay

Cells were grown in synthetic medium (0.17% yeast nitrogen base, 0.5% ammonium sulfate, amino acids to rescue auxotrophic markers except of tryptophan) supplemented with 2% glucose (SD-Trp) to logarithmic phase and OD 0.5 was harvested. A 10-fold dilution series was prepared and 3.5µl were plated on synthetic medium plates supplemented with 2% glucose (fermentable; SD-Trp) or 2% glycerol (non-fermentable; SG-Trp) and incubated at 30°C.

Analysis of protein steady state levels

Cells were grown in synthetic medium (0.17% yeast nitrogen base, 0.5% ammonium sulfate, amino acids to rescue auxotrophic markers except of tryptophan) supplemented with 2% glucose (SD-Trp) to logarithmic phase and harvested. Cells were lysed (0.1 M NaOH, 5 min; 14.000 rpm, 2min) and the pellet was re-suspended in sample buffer to extract the proteins (50 mM Tris-HCl pH 6.8, 2% SDS, 10% glycerol, 100 mM DTT; 3 min, 95°C). Samples were analyzed by SDS-PAGE (16/0.2% acrylamide/bisacrylamide) followed by transfer to nitro cellulose membranes (Roth) and subsequent immunodecoration.

Site specific photo-crosslinking

Cells were grown in SGal-Leu medium to logarithmic phase and harvested (4.400rpm, 5min, RT). ^{35}S-methionine *in vivo* labeling was performed for indicated samples as described in (19). The following steps were performed for labeled and non-labeled samples. Cells were re-suspended in SGal-Leu medium, transferred to a 6-/12-well plate and irradiated at 350 nm for 60 min (Rayonet RPR200 photochemical reactor; Edwin Gaynor 897-VS, 120W, 600V).The cells were incubated in 0.1 M NaOH (5min, RT) followed by lysis in sample buffer (50 mM Tris-HCl pH 6.8, 2% SDS, 10% glycerol, 100 mM

6

DTT) for direct analysis or with SDS (4% SDS, 100 mM DTT; 3 min, 95°C) for subsequent purification. Cbp3His7 and its crosslink products was purified by Ni-NTA (Qiagen). Samples were analyzed with SDS-PAGE (16/0.2% acrylamide/bisacrylamide) followed by transfer to nitro cellulose membranes (Roth; 90 min, 100 mA per gel) and subsequent auto-radiography or decoration with polyclonal antibodies. For antibody decoration, membranes were blocked 30 min with 5% skim-milk in TBS, incubated with primary antibody for 16h (1:500 dilution in 5% skim-milk in TBS), washed 3 times for 10 min with TBS, incubated with secondary antibody (1:10.000, anti-rabbit in 5% skim-milk in TBS), washed again 3 times for 10 min with TBS and developed with a ECL detection kit (WesternBright Quantum or WesternBright Sirius, advansta). Antibodies against Mrpl3, Mrp20, Mrpl4, Mrpl40, Qcr7, cytochrome *b* Cbp3, Cbp6, Cbp4 and Cox2 (6,7,19) were used to detect the proteins. Antibodies against Bca1 were obtained by immunizing rabbits with the recombinantly expressed and purified C-terminal domain (residues 102-482) of Bca1.

Data availability

The atomic coordinates and structure factors (code 6RWT) have been deposited in the Protein Data Bank (http://wwpdb.org).

Conflict of interest: The authors declare that they have no conflicts of interest with the contents of this article.

References:

1. Xia, D., Esser, L., Tang, W. K., Zhou, F., Zhou, Y., Yu, L., and Yu, C. A. (2013) Structural analysis of cytochrome bc1 complexes: implications to the mechanism of function. *Biochim Biophys Acta* **1827**, 1278-1294
2. Ndi, M., Marin-Buera, L., Salvatori, R., Singh, A. P., and Ott, M. (2018) Biogenesis of the *bc1* Complex of the Mitochondrial Respiratory Chain. *J Mol Biol* **430**, 3892-3905
3. Mittelmeier, T. M., and Dieckmann, C. L. (1995) *In vivo* analysis of sequences required for translation of cytochrome *b* transcripts in yeast mitochondria. *Mol. Cell. Biol.* **15**, 780-789
4. Rodel, G. (1986) Two yeast nuclear genes, CBS1 and CBS2, are required for translation of mitochondrial transcripts bearing the 5'-untranslated COB leader. *Curr Genet* **11**, 41-45
5. Gruschke, S., Kehrein, K., Römpler, K., Gröne, K., Israel, L., Imhof, A., Herrmann, J. M., and Ott, M. (2011) Cbp3-Cbp6 interacts with the yeast mitochondrial ribosomal tunnel exit and promotes cytochrome *b* synthesis and assembly. *J. Cell Biol.* **193**, 1101-1114

6. Hildenbeutel, M., Hegg, E. L., Stephan, K., Gruschke, S., Meunier, B., and Ott, M. (2014) Assembly factors monitor sequential hemylation of cytochrome *b* to regulate mitochondrial translation. *J. Cell Biol.* **205**, 511-524

7. Gruschke, S., Römpler, K., Hildenbeutel, M., Kehrein, K., Kühl, I., Bonnefoy, N., and Ott, M. (2012) The Cbp3-Cbp6 complex coordinates cytochrome *b* synthesis with *bc₁* complex assembly in yeast mitochondria. *J. Cell Biol.* **199**, 137-150

8. Tucker, E. J., Wanschers, B. F., Szklarczyk, R., Mountford, H. S., Wijeyeratne, X. W., van den Brand, M. A., Leenders, A. M., Rodenburg, R. J., Reljic, B., Compton, A. G., Frazier, A. E., Bruno, D. L., Christodoulou, J., Endo, H., Ryan, M. T., Nijtmans, L. G., Huynen, M. A., and Thorburn, D. R. (2013) Mutations in the UQCC1-interacting protein, UQCC2, cause human complex III deficiency associated with perturbed cytochrome *b* protein expression. *PLoS Genet.* **9**, e1004034

9. Perez-Martinez, X., Broadley, S. A., and Fox, T. D. (2003) Mss51p promotes mitochondrial Cox1p synthesis and interacts with newly synthesized Cox1p. *EMBO J.* **22**, 5951-5961

10. Barrientos, A., Zambrano, A., and Tzagoloff, A. (2004) Mss51p and Cox14p jointly regulate mitochondrial Cox1p expression in *Saccharomyces cerevisiae*. *EMBO J.* **23**, 3472-3482

11. Ott, M., Amunts, A., and Brown, A. (2016) Organization and Regulation of Mitochondrial Protein Synthesis. *Annu. Rev. Biochem.* **85**, 77-101

12. Remmert, M., Biegert, A., Hauser, A., and Soding, J. (2011) HHblits: lightning-fast iterative protein sequence searching by HMM-HMM alignment. *Nat Methods* **9**, 173-175

13. Johnson, L. S., Eddy, S. R., and Portugaly, E. (2010) Hidden Markov model speed heuristic and iterative HMM search procedure. *BMC Bioinformatics* **11**, 431

14. Krissinel, E., and Henrick, K. (2004) Secondary-structure matching (SSM), a new tool for fast protein structure alignment in three dimensions. *Acta Crystallogr D Biol Crystallogr* **60**, 2256-2268

15. Waterhouse, A., Bertoni, M., Bienert, S., Studer, G., Tauriello, G., Gumienny, R., Heer, F. T., de Beer, T. A. P., Rempfer, C., Bordoli, L., Lepore, R., and Schwede, T. (2018) SWISS-MODEL: homology modelling of protein structures and complexes. *Nucleic Acids Res* **46**, W296-W303

16. Chin, J. W., Cropp, T. A., Chu, S., Meggers, E., and Schultz, P. G. (2003) Progress toward an expanded eukaryotic genetic code. *Chem Biol* **10**, 511-519

17. Desai, N., Brown, A., Amunts, A., and Ramakrishnan, V. (2017) The structure of the yeast mitochondrial ribosome. *Science* **355**, 528-531

18. Amunts, A., Brown, A., Bai, X. C., Llacer, J. L., Hussain, T., Emsley, P., Long, F., Murshudov, G., Scheres, S. H., and Ramakrishnan, V. (2014) Structure of the yeast mitochondrial large ribosomal subunit. *Science* **343**, 1485-1489

19. Gruschke, S., Gröne, K., Heublein, M., Holz, S., Israel, L., Imhof, A., Herrmann, J. M., and Ott, M. (2010) Proteins at the polypeptide tunnel exit of the yeast mitochondrial ribosome. *J. Biol. Chem.* **285**, 19022-19028

20. Rathore, S., Berndtsson, J., Marin-Buera, L., Conrad, J., Carroni, M., Brzezinski, P., and Ott, M. (2019) Cryo-EM structure of the yeast respiratory supercomplex. *Nat Struct Mol Biol* **26**, 50-57

21. Gildea, R. J., Waterman, D. G., Parkhurst, J. M., Axford, D., Sutton, G., Stuart, D. I., Sauter, N. K., Evans, G., and Winter, G. (2014) New methods for indexing multi-lattice diffraction data. *Acta Crystallogr D Biol Crystallogr* **70**, 2652-2666

22. Evans, P. (2006) Scaling and assessment of data quality. *Acta Crystallogr D Biol Crystallogr* **62**, 72-82

23. Collaborative Computational Project, N. (1994) The CCP4 suite: programs for protein crystallography. *Acta Crystallogr D Biol Crystallogr* **50**, 760-763

24. Evans, P. R., and Murshudov, G. N. (2013) How good are my data and what is the resolution? *Acta Crystallogr D Biol Crystallogr* **69**, 1204-1214

25. Thorn, A., and Sheldrick, G. M. (2013) Extending molecular-replacement solutions with SHELXE. *Acta Crystallogr D Biol Crystallogr* **69**, 2251-2256

8

26. Sammito, M., Millan, C., Frieske, D., Rodriguez-Freire, E., Borges, R. J., and Uson, I. (2015) ARCIMBOLDO_LITE: single-workstation implementation and use. *Acta Crystallogr D Biol Crystallogr* **71**, 1921-1930
27. McCoy, A. J., Grosse-Kunstleve, R. W., Adams, P. D., Winn, M. D., Storoni, L. C., and Read, R. J. (2007) Phaser crystallographic software. *J Appl Crystallogr* **40**, 658-674
28. Cowtan, K. (2008) Fitting molecular fragments into electron density. *Acta Crystallogr D Biol Crystallogr* **64**, 83-89
29. Murshudov, G. N., Skubak, P., Lebedev, A. A., Pannu, N. S., Steiner, R. A., Nicholls, R. A., Winn, M. D., Long, F., and Vagin, A. A. (2011) REFMAC5 for the refinement of macromolecular crystal structures. *Acta Crystallogr D Biol Crystallogr* **67**, 355-367
30. Emsley, P., Lohkamp, B., Scott, W. G., and Cowtan, K. (2010) Features and development of Coot. *Acta Crystallogr D Biol Crystallogr* **66**, 486-501
31. Chen, V. B., Arendall, W. B., 3rd, Headd, J. J., Keedy, D. A., Immormino, R. M., Kapral, G. J., Murray, L. W., Richardson, J. S., and Richardson, D. C. (2010) MolProbity: all-atom structure validation for macromolecular crystallography. *Acta Crystallogr D Biol Crystallogr* **66**, 12-21

Table 1. X-ray crystallography: Data collection and refinement statistics

	Ba Cbp3 (PDB ID: 6RWT)
Data collection	
Space group	P $2_1 2_1 2_1$
Cell dimensions	
a, b, c (Å)	44.4, 55.9, 97.6
α, β, γ (°)	90.0, 90.0, 90.0
Resolution (Å)	1.42-44.4 (1.42-1.44)*
No. total/unique reflections	628,715 (25,672)*/ 46,643 (2242)*
R_{merge}	0.052 (1.90)*
R_{pim}	0.014 (0.57)*
$CC_{1/2}$	1.0 (0.61)*
$I / \sigma I$	18 (1.2)*
Completeness (%)	99.9 (98.0)*
Redundancy	13.5 (11.5)*
***Ab initio* phasing**	
Correlation coefficient (No. residues)	31.3% (150)
Refinement	
R_{work} / R_{free}	16.8 / 20.1
B-factors	
Protein	26.8
Mg^{2+}	34.2
Water	42.4
R.m.s. deviations	
Bond lengths (Å)	0.009
Bond angles (°)	1.18

*Values in parentheses are for highest-resolution shell.
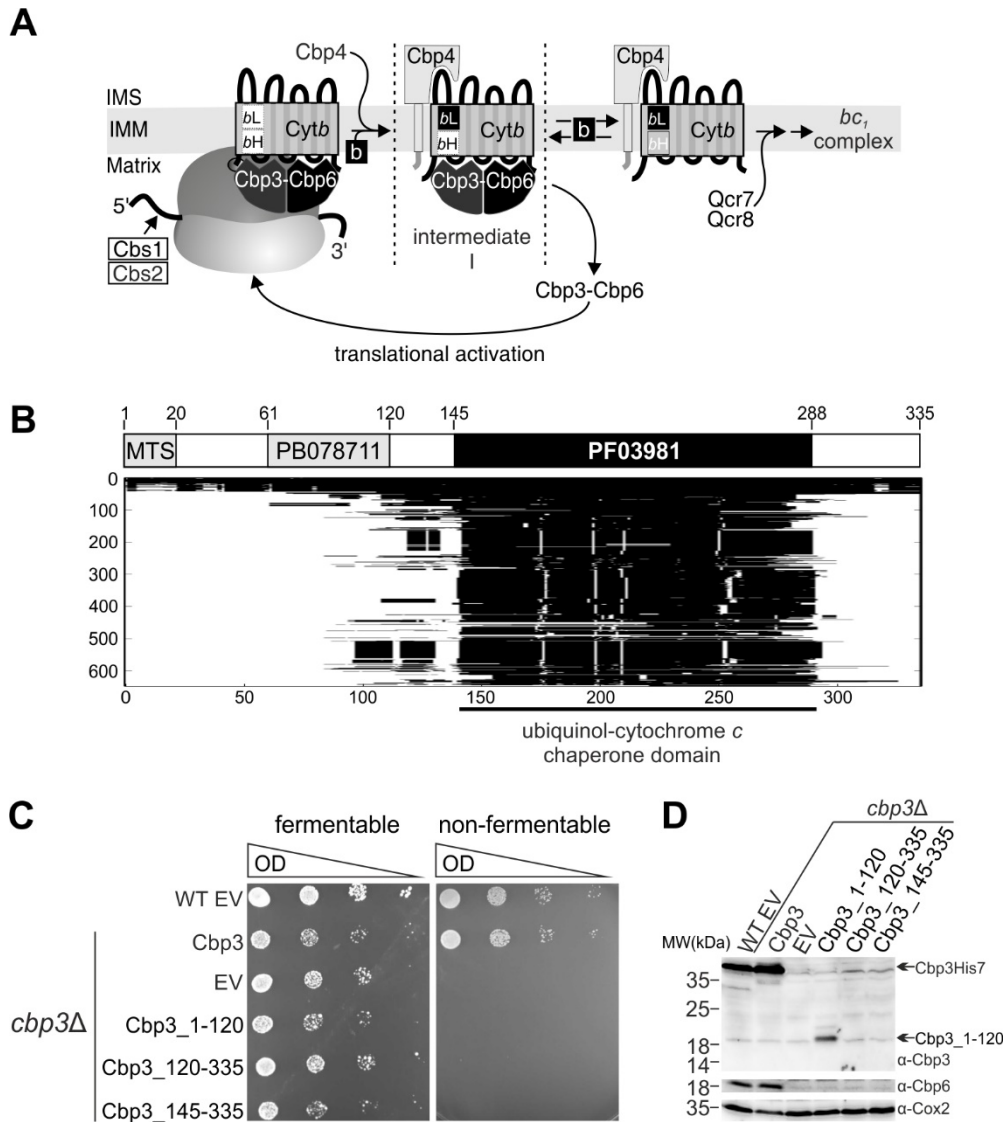
Figure 1. Bioinformatic and biochemical analysis of Cbp3 domain structure. (A) A schematic depicting the sequence of events, which take place during the early steps of cytochrome *b* biogenesis. See introduction for details. **(B)** Multiple sequence alignments generated using UniProt sequence P21560 from *Saccharomyces cerevisiae* as representative for Cbp3. The sequences in the alignment are on the Y-axis and the position of residues in the sequence on the X-axis. Black indicates alignment while white indicates gaps. The conserved ubiquinol-cytochrome *c* chaperone domain and selected residues are indicated. **(C)** Growth assay of *cbp3Δ* strains expressing either full length Cbp3 or truncated Cbp3 mutants on fermentable and non-fermentable medium at 30°C. Only the full length Cbp3 can rescue respiration in the *cbp3Δ* strain. **(D)** Protein levels of Cbp3 or its truncated mutants. The N-terminal domain is detectable but not sufficient to stabilize Cbp6 protein levels. EV, empty vector.
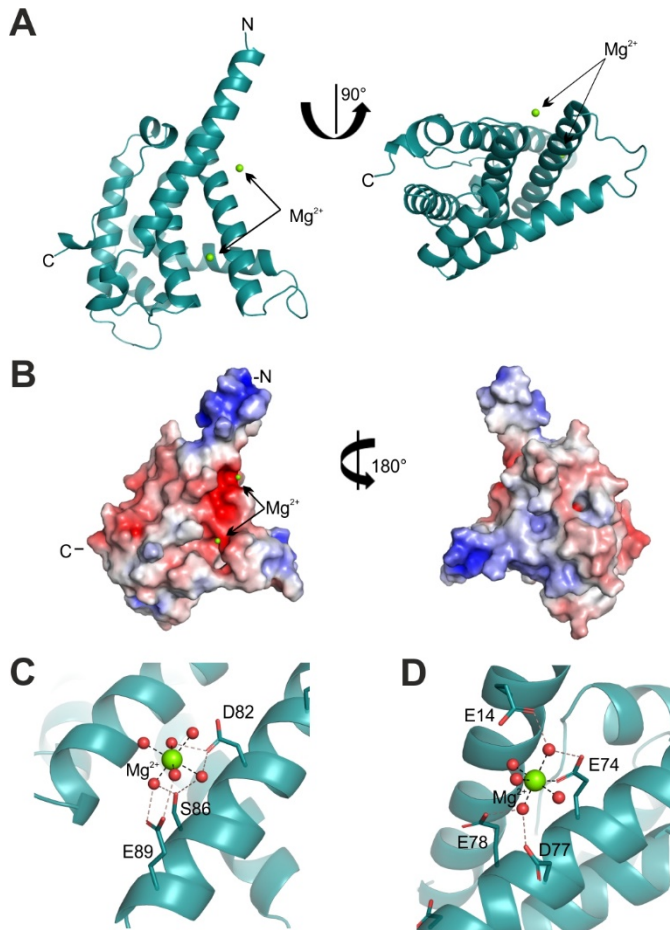
Figure 2. X-ray crystal structure of a Cbp3 homolog from *Brucella abortus*. **(A)** *Ba*Cbp3 colored in teal. The N- and C-termini are labelled and Mg^{2+} ions are shown as green spheres. **(B)** Surface potential of *Ba*Cbp3 calculated with the APBS software (from negative to positive, blue to red). **(C)** and **(D)** Magnesium ion coordination, with Mg^{2+}-coordinating bonds and water-mediated interactions shown as black and light red dashed lines, respectively. Residues involved in the interactions are highlighted.

12

Figure 3. Homology model of Cbp3 from *S. cerevisia*. (A) Sequence alignment of Cbp3 homologs from *S. cerevisiae* and *B. abortus*. Both sequences show 28.5% identity and 44.6% similarity. The numbering reflects the residues in ScCbp3 and the colouring shows the degree of conservation. (B) Crystal structure of *Ba*Cbp3 (teal) superimposed with the homology model of *Sc*Cbp3, prepared with SWISS-MODEL. The N-and C-termini of the homology model are labelled. (C) Colouring as per (B) with strictly conserved residues of the ubiquinol-cytochrome *c* chaperone family highlighted in yellow and labelled for *Sc*Cbp3. (D) Surface potential of *Sc*Cbp3 calculated with the APBS software (from negative to positive, blue to red).

Figure 4. Identification of interactions sites of *Sc*Cbp3. (A) Work-flow of UV-crosslink experiments. **(B)** Efficiency of pBpa incorporation and crosslinking upon irradiation from two individual clones carrying a TAG codon at the position R245 of *Sc*CBP3. **(C)** Locations of the residues employed for site-directed UV crosslinking of *Sc*Cbp3. Residues are highlighted in purple and their positions in the SWISS-MODEL are indicated. **(D)** UV-crosslink products of *Sc*Cbp3 at different positions decorated against Cbp3. The position of Cbp3His7 and the sizes of the crosslink products are indicated on the right. **(E)** Purification of crosslink products at specific positions and decoration with antibodies against Cbp3 and Cbp6. Cbp3His7 and the crosslink product Cbp6+Cbp3His7 are indicated. **(F)** The interaction site of Cbp3 with Cbp6 is highlighted in the Cbp3 model. Interacting residues are labelled in green. **(G)** and **(H)** Purification of crosslink products at specific positions and decoration with antibodies against Cbp3 and Cyt*b* or autoradiography of radiolabelled samples. Cbp3His7 and the crosslink product Cyt*b*+Cbp3His7 are indicated. **(I)** The interaction site of Cbp3 with Cyt*b* is highlighted in the Cbp3 model. Interacting residues are labelled in red. T, total; NB, not bound; E, elution.
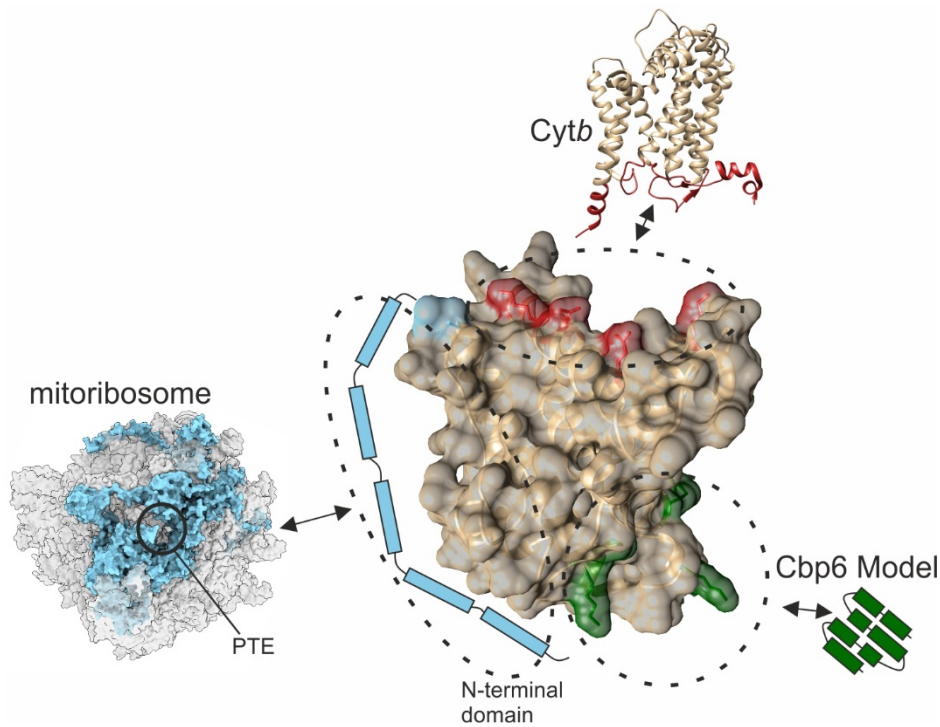
14

Figure 5. Model of interaction sites of *Sc*Cbp3. The identified interaction sites of Cbp3 with Cbp6 and Cyt*b* are indicated (green and red, respectively). The proposed interaction site of the N-terminus of Cbp3 with proteins of the peptide tunnel exit (Mrpl3, Mrpl13, Mrp20, Mrpl22, Mrpl40) of the mitoribosome is marked in blue. The model of Cyt*b* is adapted from (20) (PDB ID: 6GIQ) while the model of the mitoribosome is adapted from (17) (PDB ID: 5MRC).

Structural basis for the interaction of the chaperone Cbp3 with newly synthesized cytochrome *b* during mitochondrial respiratory chain assembly

Mama Ndi, Geoffrey Masuyer, Hannah Dawitz, Andreas Carlström, Mirco Michel, Arne Elofsson, Mikaela Rapp, Pål Stenmark and Martin Ott

Alerts:
- When this article is cited
- When a correction for this article is posted

Click here to choose from all of JBC's e-mail alerts